



Estimation Methodology of Pressure Losses in Non-circular Pipes

W. Sobieski

University of Warmia and Mazury in Olsztyn, Olsztyn, 10-900, Poland

Corresponding Author Email: wojciech.sobieski@uwm.edu.pl

ABSTRACT

The article presents a methodology for determining the hydraulic resistance multiplier, used for a rapid estimation of linear losses in pipes with non-circular cross-sections. The numerical approach was applied using the Finite Volume Method and the ANSYS Fluent software. The research was conducted under turbulent flow conditions, covering two Reynolds number ranges: 10,000 to 100,000 (10 cases) and 100,000 to 1,000,000 (5 cases). The first section of the article presents calculations of losses for a circular pipe, accompanied by a mesh test and error estimation. The second section includes calculations conducted for a series of pipes with various selected cross-sectional shapes: half-circle, quarter-circle, square, rectangles with aspect ratios of 2:1 and 3:1, isosceles triangle, and equilateral triangle. The last section of the article discusses the calculation of linear losses and the hydraulic resistance multiplier for each tested shape. It was found that this coefficient ranged from 1.33 to 2.2, depending on the shape, with the influence of the Reynolds number being relatively insignificant.

Article History

Received December 14, 2023

Revised January 19, 2024

Accepted February 14, 2024

Available online April 30, 2024

Keywords:

CFD

Numerical analysis

Hydraulic resistance multiplier

Model quality

Fit functions

1. INTRODUCTION

Estimating pressure or head losses in pipes and ducts is one of the most fundamental challenges in fluid dynamics. One of the widely used approaches is to employ the empirical Darcy-Weisbach formula (Weisbach, 1845), which is applicable to circular pipes and is expressed as follows (Brown, 2002; Cengel & Cimbala, 2018):

$$dp = \frac{\rho \cdot v^2}{2} \cdot \lambda \cdot \frac{l}{d} \quad (1)$$

where: dp – pressure loss [Pa], ρ – fluid density [kg/m^3], v – average velocity [m/s], λ – friction coefficient [-], l – length of the pipe [m], d – diameter of the pipe [m].

The friction factor plays a crucial role in Eq. (1). It can be determined through experimentation, empirical formulas (Brkić, 2011; Minhoni et al., 2020), the Nikuradse chart (Nikuradse, 1933), the Moody chart (Moody, 1944), or numerical calculations. It's important to note that its value depends on the flow regime. In the case of turbulent flow, the friction coefficient can be computed using the Blasius formula (Blasius, 1913):

$$\lambda = \frac{0.3164}{\sqrt[4]{\text{Re}}}, \quad (2)$$

where Re is the Reynolds number [-].

The literature also encompasses alternative formulas (Brkić, 2011; Minhoni et al., 2020), including the well-known Colebrook-White equation (Colebrook & White, 1937) as an illustrative example

$$\frac{1}{\sqrt{\lambda}} = -2 \log_{10} \left(\frac{\epsilon}{3.7d} + \frac{2.51}{\text{Re}\sqrt{\lambda}} \right), \quad (3)$$

where: ϵ – absolute pipe roughness [m].

The Colebrook equation can be challenging to apply as it necessitates an iterative solution to ascertain the unknown friction factor. Typically, convergence to 0.01% can be attained in fewer than 7 iterations. For practical reasons, one may opt for an explicit approximation of the implicit Colebrook equation, such as the Swamee-Jain formula (1976) (Brkić, 2011) instead:

$$\lambda = \frac{0.25}{\left[\log_{10} \left(\frac{5.74}{\text{Re}^{0.9}} + \frac{\epsilon}{3.7d} \right) \right]^2}. \quad (4)$$

When calculating the frictional head loss in non-circular pipes, the hydraulic diameter should be used instead of the internal dimensions of the pipe (He & Gotts, 2004):

$$dp = \frac{\rho \cdot v^2}{2} \cdot 4 \cdot \lambda \cdot \frac{l}{d_h}, \quad (5)$$

where: $d_h = 4A/P$ – the hydraulic diameter [m], A – the cross-sectional area of flow [m²], P – the wetted perimeter [m].

Eq. (5) can also be expressed as a function of the mass flow rate rather than the velocity

$$dp = \frac{\dot{m}^2}{2 \cdot \rho} \cdot \lambda \cdot \frac{L \cdot P}{A^3}, \quad (6)$$

where $\dot{m} = \rho A v$ is the mass flow rate [kg/s].

The methodology outlined in books (Miller, 1996) relies on the calculation of pressure drops using hydraulic diameters of channels. Eq. (6) is frequently cited, and it gives rise to the formulation of the so-called hydraulic resistance multiplier, denoted as

$$k = \frac{P_x}{P} \left(\frac{A}{A_x} \right)^3, \quad (7)$$

where x index is associated with a pipe cross-section of non-circular shape.

He and Gotts (2004) introduced a multichannel approach where a noncircular passage is partitioned into multiple subchannels, isolating the sharp corners from the central channel. Flow is permitted through all subchannels. The authors assert that their method has been successfully employed for various common geometries, yielding results typically within 5% of experimental data. The primary advantage of this method lies in its independence from experimental or numerical data.

Muzychka and Yovanovich (2009) devised a straightforward analytical model to forecast the product of the apparent friction factor and Reynolds number in non-circular ducts, particularly for emerging laminar flow. They assert that this novel model is more straightforward than other comprehensive models while delivering comparable or enhanced accuracy (within ±12%).

Frate et al. (2016) introduced a numerical approach to assess the inaccuracies in estimating friction pressure loss when applying the Darcy formula, combined with an equivalent hydraulic diameter and a friction factor valid for circular pipes, to a square rod bundle. They conducted a comparative analysis of analytical results against data from numerical simulations, revealing that errors in the range of 11% to 23% are probable when using the equivalent diameter in the laminar regime. However, in the turbulent regime, the equivalent diameter proves more effective, resulting in errors typically ranging from a few percent to approximately 12%.

Ayas et al. (2021) introduced a straightforward approximate method for estimating the friction factor of fully developed shear-thinning fluids in ducts with non-circular cross-sections during laminar flow. Their study was founded on the Metzner and Reed theory (1955) and the modified Reynolds number. The authors concluded that this method enables the determination of the friction factor with a deviation of less than 5% compared to conventional methods.

The primary objective of this investigation is to compare pressure drops in pipes with different cross-sectional shapes while maintaining constant all other

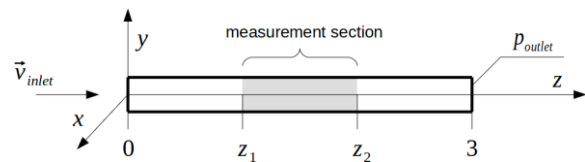


Fig. 1 The schema of the calculation space

parameters and conditions. The study was conducted based on several assumptions, as illustrated in Fig. 1. the pipe is oriented along the Z-axis; the Z-axis is positioned at the gravity center of the cross-section; the length of the pipe is consistently set at 3 meters for all cases; the cross-sectional area for each pipe is identical and equal to that of a circular pipe with a 1-inch diameter; water, with default properties in the ANSYS Fluent code (density of 998.2 kg/m³ and viscosity of 0.001003 kg/(m·s)), serves as the fluid in the simulation; the numerical model employs the Reynolds number as a key parameter, and for consistency, all calculations are conducted within the turbulent flow regime.

The water velocity at the inlet is calculated using the following formula

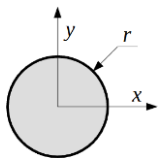
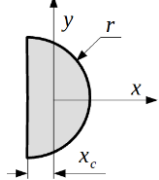
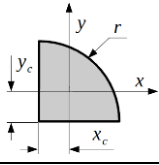
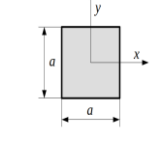
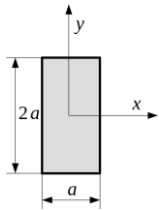
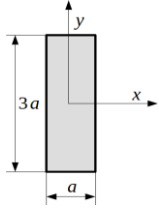
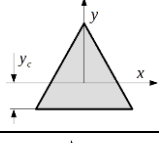
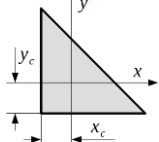
$$v_{inlet} = \frac{Re \cdot \mu}{\rho \cdot d_h} = \frac{Re \cdot \mu}{\rho \cdot \frac{4 \cdot A}{L}}, \quad (8)$$

where: v_{inlet} – the velocity at the inlet [m/s], μ – the viscosity of the fluid [kg/(m·s)], ρ – the density of the fluid [kg/m³].

Flow channels with non-circular cross-sections are found in many different industries and are often the subject of various design works (Abbas & Mohammed, 2002; Abdi et al., 2019; Khairunnisa et al., 2022). Certainly, examining every conceivable shape configuration within a single article is impractical. Nevertheless, it is feasible to introduce a relatively swift methodology aiding in the estimation of flow losses in non-circular pipes. The development of such a methodology was the main idea of the research presented in the article. The motivation for addressing the modeling of linear losses in non-circular pipes was an inquiry from the industry, which indicates that there is still a demand for this type of analysis. In this context, this research responds to a real-world need and strives to offer a valuable tool for engineers and designers working with non-circular geometries. Industries frequently encountering non-circular pipes, such as those involved in heat exchanger design, chemical processing, or specialized machinery manufacturing, stand to benefit from a more efficient and reliable approach to estimating flow losses.

The aforementioned inquiry from the industry pertained to a method for rapidly estimating pressure drops for the selection of a pump system. This selection is made during the preparation stage of a commercial offer, and as such, it cannot be overly time-consuming. Numerous such offers are prepared, with only a portion being subsequently chosen and implemented by clients. While it is always possible to include a pump system with clearly higher parameters in the offer, it will be more expensive, ultimately impacting the price. Cost overestimation

Table 1 Shapes of pipe profiles taken into account in the investigations

Case	Geometry	Formulas
a		$r = \sqrt{\frac{A}{\pi}}$ $P = 2\pi r$ $x_c = 0, y_c = 0$
b		$r = \sqrt{\frac{2A}{\pi}}$ $P = r(\pi + 2)$ $x_c = \frac{4r}{3\pi}, y_c = 0$
c		$r = \sqrt{\frac{4A}{\pi}}$ $P = r\left(\frac{\pi}{2} + 2\right)$ $x_c = \frac{4r}{3\pi}, y_c = \frac{4r}{3\pi}$
d		$a = \sqrt{A}$ $P = 4a$ $x_c = 0, y_c = 0$
e		$a = \sqrt{\frac{A}{2}}$ $P = 6a$ $x_c = 0, y_c = 0$
f		$a = \sqrt{\frac{A}{3}}$ $P = 8a$ $x_c = 0, y_c = 0$
g		$a = \sqrt{\frac{4A}{\sqrt{3}}}$ $P = 3a$ $x_c = 0, y_c = \frac{a}{2\sqrt{3}}$
h		$a = \sqrt{2A}$ $P = a(2 + \sqrt{2})$ $x_c = \frac{a}{3}, y_c = \frac{a}{3}$

is a safe approach for the company fulfilling the order but may lead to competing offers being cheaper and, ultimately, chosen by the client. Currently, the aim is to minimize cost overestimation to maintain or increase competitiveness in the market. The context described here explains why the research seeks solutions that are both fast and straightforward in implementation, yet qualitatively acceptable. It is also significant here that pump systems are selected from catalogues, and there is usually no possibility of purchasing a device with nominal parameters precisely matching those calculated in the

design. In practice, pump systems are selected with some margin in parameters, which explains why the focus in the research is on a reasonable estimation of pressure drop values rather than precise calculations considering all possible nuances. The author believes that the proposed methodology represents a good compromise between the overall quality of the simulation model and the time-consuming nature of the modelling process.

2. MATERIALS AND METHODS

2.1 The Geometry of the Calculation Space

Table 1 displays the assumed set of shapes, with the coordinate system center located at the gravity center of each shape. Since the cross-sectional area was assumed to be constant (0.000507 m²), the circle radius (r) or the polygon's side length (a) had to be calculated for each shape. In some cases, the gravity center coordinates were also required to create the geometry based on the specified assumptions. The necessary formulas are provided in Table 1, and the individual cases are identified by the letters. Table 2 provides specific data for each geometry, and Table 3 presents the inlet velocity values calculated for six chosen Reynolds numbers and all geometries, using Eq. (8).

2.2 The Finite Volume Method

In the numerical investigations, the Finite Volume Method is employed, encompassing two main types of balances: the surface balance and the volumetric balance. The surface balance delineates the exchange of a specific quantity with the surroundings through fluxes flowing across the surface of a Finite Volume. The volumetric balance describes the change of a specific value within a Finite Volume. The primary set of balance equations can

Table 2 Geometrical data of used shapes

Case	r or a	L	d _h	x _c	y _c
	[m]	[m]	[m]	[m]	[m]
a	0.0127	0.0798	0.0254	0.0	0.0
b	0.0180	0.0923	0.0219	0.0076	0.0
c	0.0254	0.0907	0.0223	0.0108	0.0108
d	0.0225	0.0900	0.0225	0.0	0.0
e	0.0159	0.0955	0.0212	0.0	0.0
f	0.0130	0.1040	0.0195	0.0	0.0
g	0.0342	0.1026	0.0198	0.0	0.0099
h	0.0318	0.1087	0.0186	0.0	0.0106

Table 3 Velocity inlet in function of the Reynolds number

	Re = (*1000)					
	10	20	50	100	500	1000
a	0.396	0.791	1.978	3.956	19.780	39.559
b	0.458	0.916	2.289	4.578	22.890	45.781
c	0.450	0.899	2.248	4.496	22.482	44.964
d	0.446	0.893	2.232	4.464	22.319	44.638
e	0.473	0.947	2.367	4.735	23.673	47.346
f	0.515	1.031	2.577	5.154	25.772	51.543
g	0.509	1.017	2.544	5.088	25.438	50.876
h	0.539	1.078	2.694	5.388	26.941	53.883

be expressed as follows (Sobieski, 2011):

$$\left\{ \begin{array}{l} \frac{\partial \rho}{\partial t} + \text{div}(\rho \vec{v}) = 0 \\ \frac{\partial(\rho \vec{v})}{\partial t} + \text{div}(\rho \vec{v} \vec{v} + p \vec{I}) = \text{div}(\vec{\tau}^l + \vec{\tau}^t) + \rho s_b \quad (9) \\ \frac{\partial(\rho e)}{\partial t} + \text{div}(\rho e \vec{v} + p \vec{I} \vec{v}) = \\ = \text{div}[(\vec{\tau}^l + \vec{\tau}^t) \vec{v} + \vec{q}^l + \vec{q}^t] + \rho s_e \end{array} \right.$$

where: ρ – density [kg/m³], \vec{v} – velocity [m/s], p – static pressure [Pa], \vec{I} – unit tensor [-], $\vec{\tau}^l$ – viscous stress tensor [Pa], $\vec{\tau}^t$ – turbulent stress tensor [Pa], s_b – source of forces [N/m³], e – sum of kinetic and internal energy [J/kg], \vec{q}^l – laminar heat flux [J/(m²s)], \vec{q}^t – turbulent heat flux [J/(m²s)], s_e – sources of heat [J/(m³s)].

The equations in set (9) comprise the mass balance equation and momentum balance equation. Thermal issues are not considered, so the energy balance equation is not used in this study. It is important to note that the set of balance (or transport) equations (9) is incomplete and necessitates additional "closure" models to describe individual problems (Sobieski, 2013). Specifically, the evolution equations must be introduced to determine parameters used in turbulence modeling should be added. In the case of the k- ω SST model, these equations take the form (ANSYS inc., 2022a):

$$\frac{\partial(\rho k)}{\partial t} + \frac{\partial(\rho k v_i)}{\partial x_j} = \frac{\partial(\Gamma_k \frac{\partial k}{\partial x_j})}{\partial x_j} + G_k - Y_k + G_b. \quad (10)$$

and

$$\frac{\partial(\rho \omega)}{\partial t} + \frac{\partial(\rho \omega v_i)}{\partial x_j} = \frac{\partial(\Gamma_\omega \frac{\partial \omega}{\partial x_j})}{\partial x_j} + G_\omega - Y_\omega + D_\omega + G_{\omega b}. \quad (11)$$

where: G_k – term representing the production of turbulence kinetic energy, G_ω – term representing the generation of ω , Γ_k and Γ_ω – terms representing the effective diffusivity of k and ω , Y_k and Y_ω – terms representing the dissipation of k and ω due to turbulence, D_ω – term representing the cross-diffusion phenomenon, G_b and $G_{\omega b}$ – terms representing the buoyancy account.

3 RESULT AND DISCUSSION

3.1 Settings of the Numerical Model

All numerical models were created using ANSYS Fluent code, version 2022R1. The geometries were modeled based on the data provided in Section 1 and Section 2.1. The so-called sweep numerical mesh was generated for all eight geometries with a manually defined source, which was always the surface representing the velocity inlet. The element size was set to 0.0015 [m]. An inflation mesh added to the pipe walls in each case. To generate the inflation layer, the smooth transition method was employed with a transition ratio set to 0.272. The number of layers was configured to 5, and the growth rate was set to 1.2. The number of cells was approximately three million for each geometry. The orthogonality factor ranged from 0.34 to 0.71, and the skewness ranged from

0.5 to 0.79 depending on the case, indicating very good mesh quality. The worst mesh quality indicators were obtained for sections with triangular shapes.

The calculations were performed using the steady-state solver with standard parameters and the k- ω SST turbulence model. Water density and viscosity were set according to the assumptions mentioned in the introduction. The inlet velocity was determined from the data provided in Table 3. To determine the turbulence parameters at the inlet, the option requiring the input of the hydraulic diameter, as seen in Table 2, and the turbulence intensity parameter was chosen. Generally, it is considered that this parameter for internal flows should be within the range of 1 or 2% (depending on the source) to 5%. To assess the impact of this parameter, two simulations were conducted for a circular pipe with Reynolds number $Re = 20000$. It was found that when changing the turbulence intensity from 2% to 5%, the difference in pressure drop was only 0.019 [Pa]. Therefore, it was concluded that this parameter is insignificant, and the lower of the two values was adopted. It is worth to note that this parameter pertains to the inlet, while the pressure drop measurement was taken far from it. This may explain why no significant differences were observed in the described test. The relative pressure at the pressure outlet was set to zero, indicating atmospheric pressure.

To minimize the number of simulations, the subsequent studies were based on 14 selected Reynolds numbers, divided into two ranges. The first range, referred to as the low range, covered Reynolds numbers ranging from 10,000 to 100,000 in increments of 10,000. The second range, referred to as the high range, covered Reynolds numbers ranging from 100,000 to 1,000,000 in increments of 250,000. The Reynolds number of 100,000 was included in both ranges.

In the initial convergence tests conducted on the case of a circular pipe with $Re = 20000$, a uniform convergence criterion of $1e-07$ was adopted for all variables. Later, in an attempt to reduce the overall task execution time, this criterion was adjusted to a value of $1e-05$. It turned out that the pressure difference changed only by 0.002 [Pa]. It was also observed that the mass flow rate imbalance changed from $3.32e-10$ [kg/s] to $-1.11e-07$ [kg/s]. Another distinction between the two simulations was that changing the convergence criterion from $1e-07$ to $1e-05$ reduced the computation time for the tested case from about 60 minutes to about 40 minutes. Taking all these factors into account, it was concluded that a convergence criterion of $1e-05$ is sufficient, and this value was applied in all subsequent simulations. The calculations were initialized using the hybrid method and assumed 1000 iterations, although convergence was achieved much earlier. For example, for $Re = 20000$ and cases from a to h, convergence was achieved after 184, 186 ($7.1118e-07$), 135 ($-8.7165e-07$), 116 ($-2.7128e-05$), 154 ($-1.9622e-05$), 128 ($1.0372e-05$), 117 ($1.1638e-06$), and 120 ($2.7142e-06$) iterations, respectively. In parentheses, the value of mass flow rate imbalance at the inlet and outlet of the pipeline is provided.

Calculations were performed in a single process,

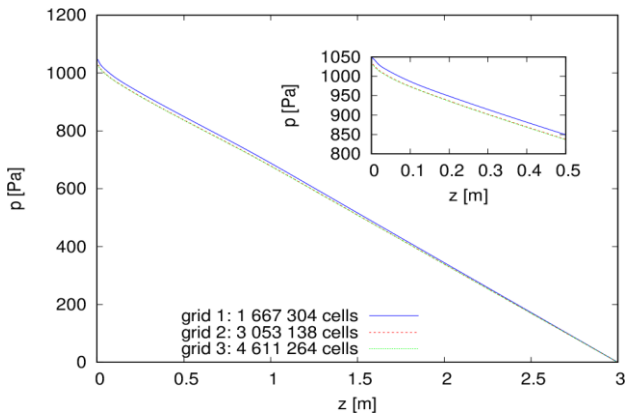


Fig. 2 Pressure drops for the circular pipe and three numerical grids

using double precision mode, on a computer with the following specifications: Intel Core i7-4930K CPU 3.4 GHz, 32.0 GB RAM, Windows 10 Pro x64. The actual computation time varied depending on the case, ranging from approximately 40 to about 60 minutes.

3.2 Grid Test

Before the main calculation step, a grid test was conducted for the standard geometry, which is the case with a circular pipe. By adjusting the "element size" parameter in the global mesh settings, three different grids were generated, with cell counts of 1,667,304, 3,053,138, and 4,611,264. The test was conducted at a Reynolds number of 20,000, and the calculation results are depicted in Fig. 2.

It can be observed that the pressure drop for the sparser grid is slightly higher than for both denser grids. Finally, it was concluded that the second grid is sufficient to achieve the main research objective. As mentioned earlier, the remaining grids were created to always have a cell count of approximately 3 million cells.

3.3 The Measurement Section

In Fig. 2, it can be observed that the pressure drop is higher at the beginning section of the pipe. This is because a constant inlet velocity value was defined across the entire inlet surface. To obtain representative pressure drop values, the measurement section should be located at a point where the velocity profile has fully stabilized. Figure 3 shows a comparison of velocity profiles in the ZY plane. It can be observed that the profiles are the same for $z = 1.5$, 2.0 , and 2.5 . Therefore, the measurement section should be located between $z_1 = 1.5$ m and $z_2 = 2.5$ m. Velocity profiles were also obtained for much higher Reynolds numbers (Fig. 4), but the conclusion remains the same. It is assumed here that this location of the measuring section will also be applicable for other pipe geometries.

The problem of an incorrect velocity profile could be solved by setting an appropriate velocity distribution at the inlet. Unfortunately, even in the case of pipes with a circular cross-section, there are many calculation formulas (Štigler, 2014), and it is difficult to select them without the appropriate experimental data. In the case of other shapes, the difficulties in describing the inlet profile are even greater. This explains why this approach was not used in the article.

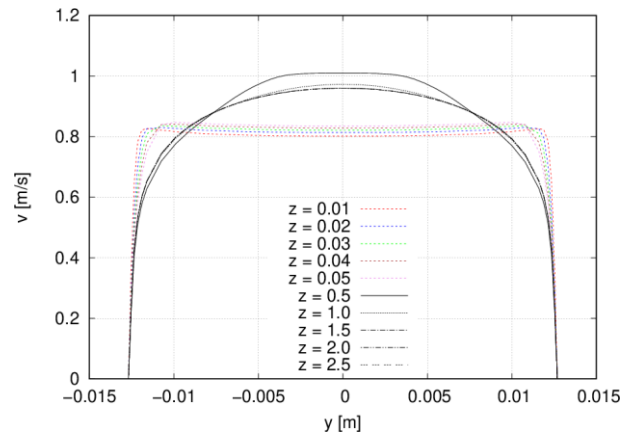


Fig. 3 Velocity profiles for circular pipe and $Re = 20000$

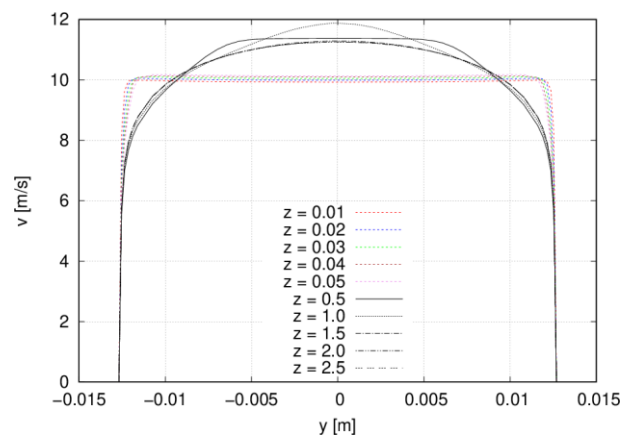


Fig. 4 Velocity profiles for circular pipe and $Re = 250000$

The conclusion reached is consistent with the existing literature. In the case of turbulent flow, the length of the entrance region in a circular pipe can be estimated using the following formula (Cengel & Cimbala, 2018)

$$L_{er} = 1.359 \cdot D \cdot Re^{0.25}, \quad (12)$$

where: L_{er} – the length of the entrance region [m], D – the diameter of the pipe [m], Re – the Reynolds number [-]. For the highest Reynolds number considered, the length of the entrance region is 1.092 [m]. This confirms that the selected measurement section is appropriate.

3.4 The Quality Test of the Numerical Model

The results of calculations for the circular pipe and both ranges of Reynolds numbers are shown in Figs 5 and 6. The numerical results obtained were also compared with an analytical solution based on Eq. (1), using the inlet velocity as the average velocity. The friction factor was calculated using Eq. (2).

It can be observed that the relative error (depicted in the inner plots) is relatively small and usually does not exceed 4%. While other analytical methods could be considered, the discussion about choosing the best empirical formula is not the aim of this paper. It is assumed here that the numerical model's accuracy is adequate to correctly calculate the pressure drops and make relative comparisons between the results.

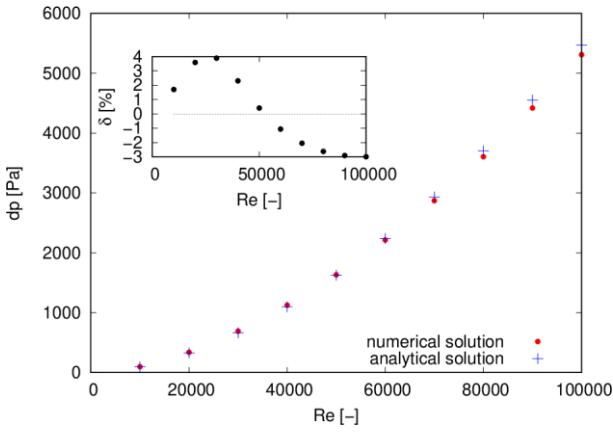


Fig. 5 Comparison of results for circular pipe, low Reynolds number range and the numerical and the analytical solution

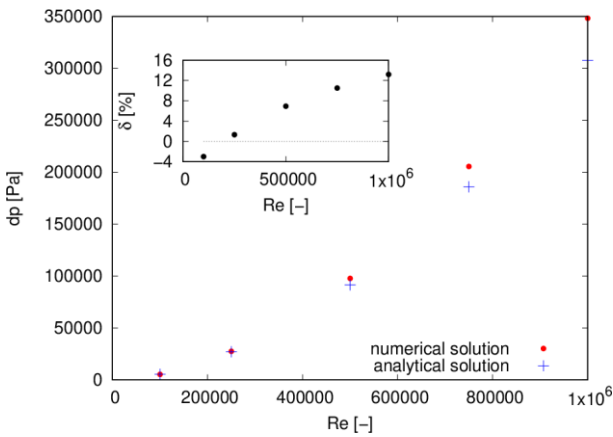


Fig. 6 Comparison of results for circular pipe, high Reynolds number range and the numerical and the analytical solution

In Fig. 6, it can be observed that the relative error clearly increases with the Reynolds number value. Perhaps the reason for this lies in the fact that the same numerical mesh was used in all calculations, and the y^+ parameter values were not taken into account. It was suggested here that the $k-\omega$ SST model is relatively

insensitive to this parameter [ANSYS inc., 2022a]. However, for such a wide range of Reynolds numbers, it may be advisable to modify the numerical mesh, for example, by changing the parameters of the inflation layer generation. Ultimately, it was decided not to take this step in order to avoid complicating the methodology, making the estimation of pressure drops simpler and faster to perform.

In further studies, it was assumed that a change in the shape of the pipe cross-section would not lead to a significant deterioration in the quality of the numerical model, as long as all other settings and parameters of the model remain unchanged. It was also assumed, that a change in the shape of the pipe cross-section would not result in the occurrence of bifurcation phenomena that would cause a significant change in the flow character, affecting the obtained values of the pressure drop.

If we compare the turbulence intensity distributions for a selected case, here for a circular pipe at $Re = 20000$ with a cross-section located 2 [m] from the inlet (Fig. 7), it turns out that there are indeed certain differences, both in terms of values range and spatial distribution. It can be assumed that similar or even greater variations will be observed for other shapes and Reynolds numbers. Therefore, it is important to be aware that the turbulence intensity value will be significant, for example, when attempting to numerically reproduce experimentally determined velocity profiles, pressures, etc. Since such data is not available here, and the context of the article is different, this aspect was not taken into account in further studies. Alternatively, instead of applying a single chosen turbulence intensity value at the inlet, as in the described studies, a general formula for estimating this parameter can be used (to obtain percentage values, the obtained result should be multiplied by 100) (ANSYS inc., 2022a):

$$I_{\%} = 0.16 \cdot Re^{-(1/8)}. \tag{13}$$

This approach was not utilized in the research because, for the considered range of Reynolds numbers, the results fall within the range of 2-5%, which aligns with the values described in subsection 3.1 of the test regarding the influence of this parameter on the calculated pressure drops.

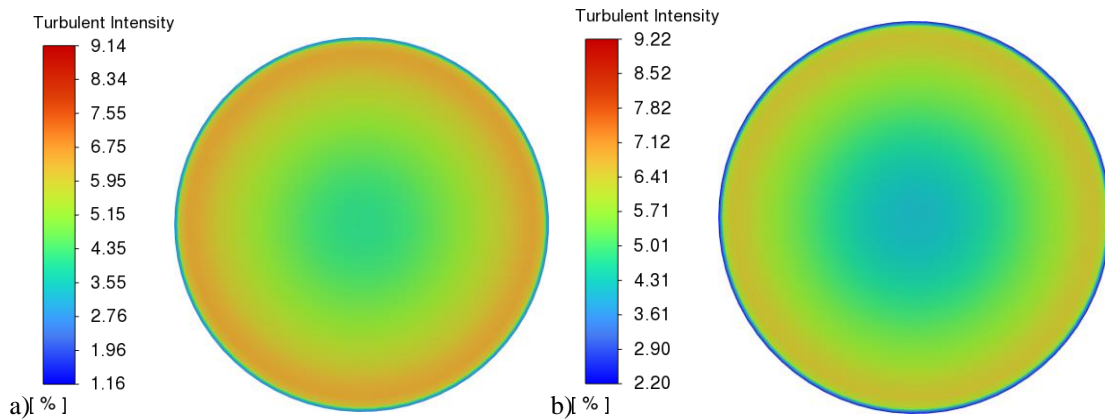


Fig. 7 Comparison of contours of the turbulence intensity for circular pipe, $Re = 20000$, $z = 2.0$ [m] and turbulent intensity at the inlet set to: a) 2%, b) 5%

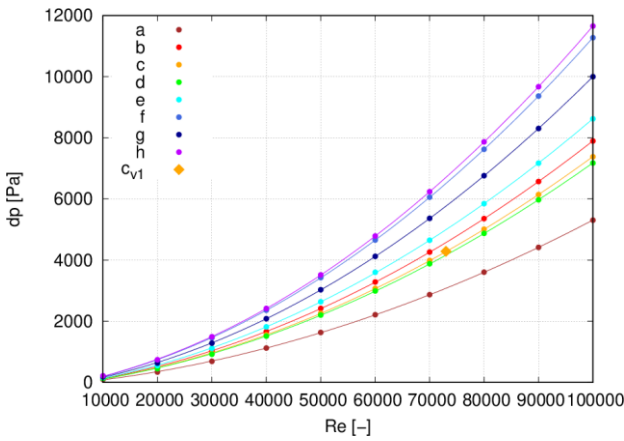


Fig. 8 Pressure drops for all geometries and low range of Reynolds numbers

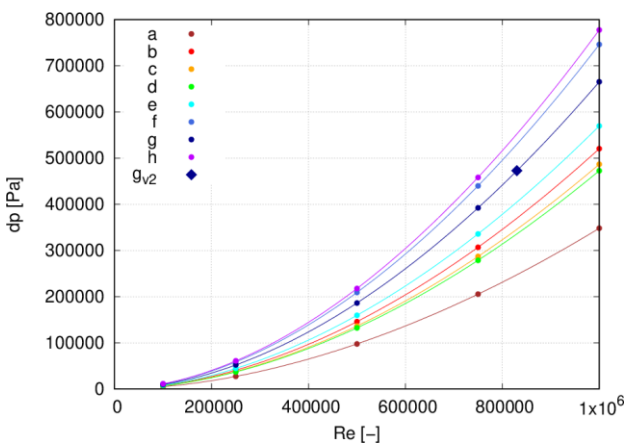


Fig. 9 Pressure drops for all geometries and high range of Reynolds numbers

During the tests investigating the impact of turbulence intensity on the results, the value of the parameter y^+ near the wall was also examined at cross-sections located 1.5 and 2.5 meters from the inlet, which represent the beginning and end of the measurement section. The value of y^+ was 3.5 for both examined cases. Additionally, the value of y^+ was checked for the circular pipe and the case with the highest Reynolds number. The obtained result of y^+ is equal to 120.

3.5 Comparison of Pressure Drops

After determining the necessary mesh resolution, the location of the measurement section, and estimating the accuracy of the numerical model, the main simulations were conducted. The results of the calculations are presented in Figs 8 and 9. It is apparent that the circular pipe generates the least flow resistance, followed by the square pipe and the pipe with a quarter-circle cross-section, where pressure drops are relatively similar. The half-circle cross-section pipe generates a slightly greater pressure drop, while rectangular pipes generate greater resistance. The resistances increase with the greater ratio of the lengths of the sides of the rectangle.

The greatest resistance is generated by pipes with triangular cross-sections due to the existence of sharp

Table 4 Velocity value distribution in the XY plane, for $Re = 20000 [-]$ and $Z = 2.0 [m]$ (cross-sections are not in the same scale)

$v_{max} = 1.046$	$v_{max} = 1.203$	$v_{max} = 1.206$	$v_{max} = 1.203$
a	b	c	d
$v_{max} = 1.230$	$v_{max} = 1.305$	$v_{max} = 1.393$	$v_{max} = 1.474$
e	f	g	h

corners with low flow velocities (see Table 4). This reduces the effective cross-section of the conduit, increases the velocity along the pipe axis, and consequently causes higher shear rates and higher viscous friction. This is further supported by the maximum velocity values in Table 4 in lines 3 and 6.

The greater the maximum velocity value, the smaller the effective cross-sectional area of the fluid stream. The ratio of the maximum velocity in a non-circular tube to the corresponding value calculated for a circular tube is 1.151, 1.153, 1.150, 1.176, 1.248, 1.332, 1.41, for cases b to h, respectively. The description of points c_{v1} and g_{v2} is discussed in subsection 3.6.

In the scenario where the areas of two cross-sections are identical, the hydraulic resistance multiplier (as per Eq. (7)) takes the following form

$$k = \frac{dp_i}{dp_a} \tag{14}$$

where: dp_i – the pressure drop for the i -th geometry (cases from b to h) [Pa], dp_a – the pressure drop for circular pipe (case a) [Pa].

In the low Reynolds number group (Fig. 10), the hydraulic resistance multiplier varies from approximately 1.33 to about 2.2, contingent on the shape and the Reynolds number's value. In the high Reynolds number group (Fig. 11), this coefficient maintains a similar order of magnitude. It is noticeable that the hydraulic resistance multiplier exhibits only a minor dependence on the Reynolds number. This clarifies why the article does not extensively address turbulence modeling issues. Table 5 provides the average values of the hydraulic resistance

Table 5 Average values of the hydraulic resistance multiplier

	k_{b-a}	k_{c-a}	k_{d-a}	k_{e-a}	k_{f-a}	k_{g-a}	k_{h-a}
1	1.484	1.386	1.346	1.619	2.116	1.869	2.176
2	1.492	1.395	1.354	1.632	2.137	1.902	2.221
3	1.486	1.388	1.348	1.623	2.123	1.880	2.191

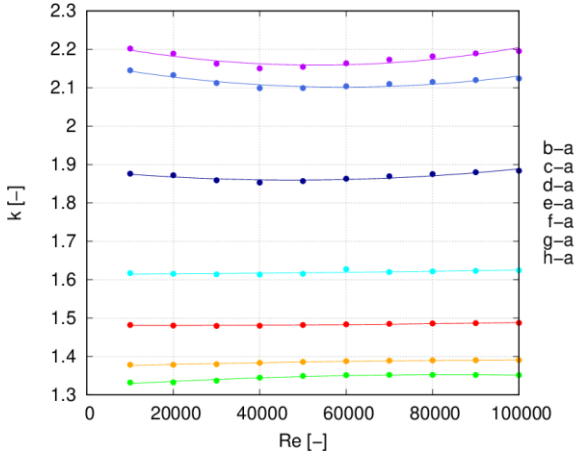


Fig. 10 The hydraulic resistance multiplier for all geometries and low range of Reynolds numbers

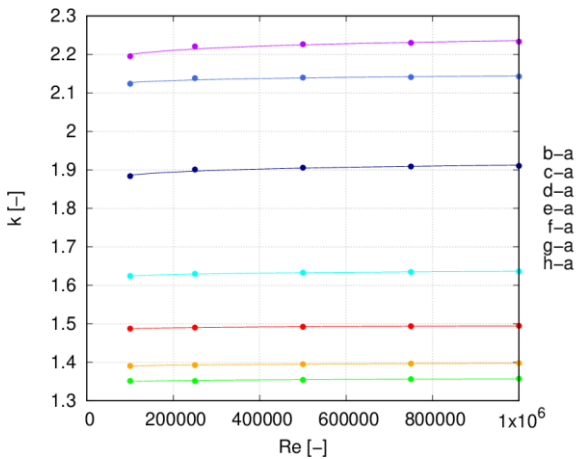


Fig. 11 The hydraulic resistance multiplier for all geometries and high range of Reynolds numbers

multiplier for the low, high, and the entire range of Reynolds numbers.

Based on the acquired data, the following approximation functions can be suggested for both low:

$$k_{b-a} = \frac{1.05682}{10^{12}} \cdot Re^2 - \frac{3.15833}{10^8} \cdot Re + 1.4812, \quad (15)$$

$$k_{c-a} = -\frac{1.24242}{10^{12}} \cdot Re^2 + \frac{2.96121}{10^7} \cdot Re + 1.37409, \quad (16)$$

$$k_{d-a} = -\frac{4.2197}{10^{12}} \cdot Re^2 + \frac{7.11621}{10^7} \cdot Re + 1.32282, \quad (17)$$

$$k_{e-a} = \frac{7.12121}{10^{13}} \cdot Re^2 + \frac{3.57879}{10^8} \cdot Re + 1.6145, \quad (18)$$

$$k_{f-a} = \frac{1.72917}{10^{11}} \cdot Re^2 - \frac{2.04275}{10^6} \cdot Re + 2.16177, \quad (19)$$

$$k_{g-a} = \frac{1.07235}{10^{11}} \cdot Re^2 - \frac{1.02358}{10^6} \cdot Re + 1.88381, \quad (20)$$

$$k_{h-a} = \frac{2.09583}{10^{11}} \cdot Re^2 - \frac{2.23311}{10^6} \cdot Re + 2.21814, \quad (21)$$

and high Reynolds numbers:

$$k_{b-a} = 1.45237 \cdot Re^{0.00207923}, \quad (22)$$

$$k_{c-a} = 1.35475 \cdot Re^{0.00225794}, \quad (23)$$

$$k_{d-a} = 1.31916 \cdot Re^{0.00204426}, \quad (24)$$

$$k_{e-a} = 1.56749 \cdot Re^{0.00311332}, \quad (25)$$

$$k_{f-a} = 2.04214 \cdot Re^{0.00352593}, \quad (26)$$

$$k_{g-a} = 1.76154 \cdot Re^{0.00594982}, \quad (27)$$

$$k_{h-a} = 1.76154 \cdot Re^{0.00594982}. \quad (28)$$

In equations (15)-(21), the coefficients associated with the Reynolds number are very small, resulting in a minor impact of this parameter on the hydraulic resistance multiplier. A slight influence of the Reynolds number can also be observed in equations (22)-(28), where the small value of the exponent indicates that this term is close to unity.

3.6 Validation Test

To determine the suitability of pressure drop estimation based on approximation functions, three additional simulations (validation tests) were performed: 1) for a pipe with a quarter-circle cross-section (geometry c) and $Re = 73000$; 2) for a pipe with an equilateral triangle cross-section (geometry g) and $Re = 83000$; 3) for a pipe with a rectangle cross-section with a side ratio of 1:3 (geometry f) and $Re = 64000$. In the first two cases, the cross-sectional area remained the same as before, while in the third case, it was altered. It was assumed that the rectangle has dimensions of 0.02 by 0.06 [m], resulting in a cross-sectional area of 0.0012 [m²]. In the case of tests No. 1 and 2, it was sufficient to change the inlet velocity in the already developed models. The obtained pressure drops, denoted as c_{v1} and g_{v2} , were added to Figs 8 and 9, respectively. For test No. 3, the simulation model was created anew, applying the same principles as before.

In the case of test 1, the hydraulic resistance multiplier was calculated using equation (16). For the assumed Reynolds number the value of this parameter is equal to 1.3891. The theoretical pressure drop in the reference pipe with a circular cross-section, calculated based on equations (1) and (2), was 3154.31 [Pa]. Using equation (14), it can be estimated that the unit pressure drop in validation test 1 should be approximately 4381.61 [Pa]. In turn, the value of the unit pressure drop obtained from numerical simulation was 4289.07 [Pa], resulting in a relative estimation error of -2.16%.

Table 6 Characteristics of individual methodologies

a)	<p>Analytical solution based on the Darcy-Weisbach equation. Friction factor calculated using the Blasius formula. Result depends on the Reynolds number. In each shape, an arbitrarily adopted constant (a) determines the size of the corner. The method considers only symmetric shapes, where the constant defining the size of all corners is the same for a given shape. Considered shapes include: square duct, equilateral triangle, arrowhead passage, rods-flat plates flow passage, tube bundles – corner tube bundles – side, tube bundles – centre.</p>
b)	<p>Analytical solution based on the Fanning friction factor. Instead of the hydraulic resistance multiplier, the authors calculate the incremental pressure drop. The result depends on the Reynolds number. The calculations utilize the so-called aspect ratio. Considered shapes include: triangle (in 3 variants), square, pentagon, hexagon, circle, semi-circle, rectangle (with different ends), ellipse, hyper-ellipse, sinusoid, circular sector, annular sector, rhombus, trapezoid.</p>
c)	<p>Analytical solution based on the Darcy-Weisbach equation (divided into laminar and turbulent regimes) and numerical solution based on the mass balance equation and momentum balance equation (using CFX and NEPTUNE_CFD programs). The authors analyse a chosen shape: a channel with a square cross-section with four circular cut-outs representing pipes placed in the channel. The authors mention the hydraulic resistance multiplier but directly calculate and compare pressure drops. Numerical simulations are performed twice: once for the entire cross-section and once for 1/8 of the cross-section. The method requires access to specialized CFD software and the necessity to learn its operation.</p>
d)	<p>Analysis solely focuses on fully developed laminar flows. Analytical solution based on the Fanning friction factor. The result depends on the Reynolds number (using various formulas for its calculation). Pressure drops are not calculated, and the hydraulic resistance multiplier is not utilized in the work. A lot of attention is given to the flow index. Considered shapes include: concentric annuli, rectangular, isosceles triangle, ellipse, symmetrical L-shape, eccentric annulus, square duct with a centred cylindrical core.</p>
e)	<p>Numerical solution based on the mass balance equation and momentum balance equation (using the ANSYS Fluent program). In the validation test performed for a circular pipe, the Darcy-Weisbach equation is applied, with the</p>

<p>friction factor calculated from the Blasius formula. The result depends on the Reynolds number. Each shape is analysed in the same way. No model constants related to the geometry of a given shape The method requires access to specialized CFD software and the necessity to learn its operation. Considered shapes include: circle, semicircle, quarter circle, square, rectangle (in 2 variants), triangle (in two variants).</p>

In validation test number 2, it was calculated that the hydraulic resistance multiplier is equal to 1.9103. Equation (27) was applied in this case. The unit pressure drops were 424215.22 [Pa] and 472828.00 [Pa], respectively, for the estimation from the approximation function and the numerical simulation. The relative error in this case was 10.28%, which is still not a bad result.

In validation test number 3, the approximation function (19) was utilized, yielding $k = 2.1019$. The unit pressure drop calculated for a circular pipe with the same cross-sectional area as the tested pipe was estimated at 1445.02 [Pa]. The pressure drop obtained from numerical simulation was 1449.06 [Pa]. The relative error in this case was 0.28%, which is highly satisfactory.

It can be argued that the approximation functions developed for lower Reynolds numbers, equations (15)-(21), allow for estimating pressure drops at a level of a few percent. On the other hand, the accuracy of the approximation functions obtained for higher Reynolds numbers, equations (22)-(28), is at the level of several percent. It can be roughly assumed that the quality of the estimation is adequate to the quality of the simulation model (see errors in Figs 5 and 6).

3.7 Comparison with the Other Methods

The computational methods described in the cited works in the introduction differ significantly from those proposed in this article. In particular, there is no possibility of quantitatively comparing individual results. Nevertheless, to emphasize the uniqueness of the proposed methodology, the characteristics of each concept have been summarized in Table 6. It is worth noting that the majority of predecessors' works focus on the friction factor rather than pressure drops. The methodology proposed in the article requires the use of specialized software but is highly versatile and applicable to any shape without the need for uncertain empirical formulas or additional geometric indicators. An advantage is also the use of full conservation equations rather than selected analytical formulas. Although other methods, such as the one proposed in the work by He & Gotts (2004), may be relatively simple to implement, their use still requires a significant amount of effort. Therefore, creating a simulation model seems to be a good alternative, offering much greater possibilities, flexibility, and future potential. It is worth adding that the use of commercial software is not necessary, and the task could be accomplished using, for example, OpenFOAM, which would not incur additional costs. The individual rows of table 6 refer to the

following methodologies: a) He and Gotts (2004); b) Muzychka and Yovanovich (2009); c) Frate et al. (2016); d) Ayas et al. (2021); e) this paper.

4. CONCLUSION

The conducted research illustrates a method that allows for a relatively quick assessment of pressure drops in pipes with various non-circular cross-sections. Two approaches, a simplified and a more accurate one, are possible. In the simplified approach, the process involves two steps: first, calculating the pressure drop in a circular pipe with an equivalent cross-sectional area to the tested pipe (assuming identical fluid parameters and the same Reynolds number), and then multiplying the result by the appropriate hydraulic resistance multiplier for the specific shape. At this stage, either a constant value (refer to Table 5) or a function where the hydraulic resistance multiplier depends on the Reynolds number (Equations 15-28) can be employed. If the multiplier for a given shape is not available, the article proposes a method to determine it through two numerical simulations: one for a circular cross-section and another for the specific shape under investigation. It's crucial to ensure the fulfillment of the assumptions listed in Section 1 during the simulations. Results from both simulations can then be utilized to calculate a specific hydraulic resistance multiplier valid for the considered case.

The comparative analysis method for a unitary pipe length is more convenient and much faster than conducting numerical calculations for the entire geometries of various structures, such as helical tubes, heat exchangers, or other elements utilizing channels with non-circular shapes.

The described approach, especially the second option, holds particular appeal for applications in the industry, where similar components are frequently manufactured with variations in details, such as the length of the flow channel. Once the resistance coefficient is determined, it can be applied consistently across multiple subsequent projects.

ACKNOWLEDGEMENTS

This study was funded by the Polish Ministry of Science and Higher Education within the framework of the University's statutory research.

CONFLICT OF INTEREST

I have no financial or non-financial interests or relationships that could pose a conflict of interest with respect to the submitted manuscript.

REFERENCES

Abbas, A. S., & Mohammed, A. A. (2022). Augmentation of plate-fin heat exchanger performance with support of various types of fin configurations. *Mathematical Modelling of Engineering Problems*, 9(5), 1406-1414. <https://doi.org/10.18280/mmep.090532>

- Abdi, H., Asaadi, S., Kivi, H. A., & Pesteei, S. M. (2019). A comprehensive numerical study on nanofluid flow and heat transfer of helical, spiral and straight tubes with different cross sections. *International Journal of Heat and Technology*, 37(4), 1031-1042. <https://doi.org/10.18280/ijht.370412>
- ANSYS inc. (2022a) Ansys Fluent Theory Guide, Release 2022R1, January 2022.
- ANSYS inc. (2022b) Ansys Fluent User's Guide, Release 2022R1, January 2022.
- Ayas, M., Skocilas, J., & Jirout, T. (2021). Friction factor of shear thinning fluids in non-circular ducts – a simplified approach for rapid engineering calculation, *Chemical Engineering Communications*, 208(8), 1209-1217. <https://doi.org/10.1080/00986445.2020.1770232>
- Blasius, P. R. H. (1913). *Das aehnlichkeitsgesetz bei reibungsvorgangen in flüssigkeiten* (in German). *Forschungsheft* 131, 1-41.
- Brkić, D. (2011). Review of explicit approximations to the Colebrook relation for flow friction. *Journal of Petroleum Science and Engineering*, 77(1), 34-48. <http://dx.doi.org/10.1016/j.petrol.2011.02.006>
- Brown, G. G. (2002, November 3-7). *The history of the darcy-weisbach equation for pipe flow resistance*. Environmental and Water Resources History Sessions at ASCE Civil Engineering Conference and Exposition, Washington, D. C., United States. [http://dx.doi.org/10.1061/40650\(2003\)4](http://dx.doi.org/10.1061/40650(2003)4)
- Cengel, Y. A., & Cimbala, J. M. (2018). *Fluid Mechanics – Fundamentals and applications*. 3rd ed. McGraw-Hill, New York.
- Colebrook, C. F., & White, C. M. (1937). Experiments with Fluid Friction Factor in Roughened Pipes. *Proceedings of the Royal Society of London. Series A: Mathematical and Physical Sciences*, 161, 367-381. <http://dx.doi.org/10.1098/rspa.1937.0150>
- Frate, L., Moretti, F., Galassi, G., & D'Auria, F. (2016). Limitations in the use of the equivalent diameter. *World Journal of Nuclear Science and Technology*, 6, 53-62. <http://dx.doi.org/10.4236/wjnst.2016.61005>
- He, S., & Gotts, J. A. (2004). Calculation of friction coefficients for noncircular channels. *Journal of Fluids Engineering*, 126, 1033-1038. <https://doi.org/10.1115/1.1845479>
- Khairunnisa, N., Arifin, Z., Kristiawan, B., Hijriawan, M., & Prasetyo, S. D. (2022). Investigation of spirals rectangular and rectangular tubes collector design in photovoltaic solar cell cooling systems. *International Journal of Heat and Technology*, 40(6), 1359-1365. <https://doi.org/10.18280/ijht.400602>
- Miller, D. S. (1996). *Internal flow systems*, 2nd ed., BHR Group Limited, Bedfordshire, UK.
- Moody, L. F. (1944). Friction factors for pipe flow.

Transactions of the ASME, 66(8), 671-684.

- Minhoni, R., Pereira, F., Silva, T., Castro, E., & Saad, J. (2020). The performance of explicit formulas for determining the Darcy-Weisbach friction factor. *Engenharia Agrícola*, 40(2), 258-265. <https://doi.org/10.1590/1809-4430-eng.agric.v40n2p258-265/2020>
- Muzychka, Y., & Yovanovich, M. (2009). Pressure drop in laminar developing flow in noncircular ducts: A scaling and modeling approach. *Journal of Fluids Engineering*, 131(11), 111105. <https://doi.org/10.1115/1.4000377>
- Nikuradse, J. (1933). *Strömungsgesetze in rauen rohren*. Forschungsheft, Berlin.
- Sobieski, W. (2011). The basic equations of fluid mechanics in form characteristic of the finite volume method. *Technical Sciences*, 14(2), 299-313.
- Sobieski, W. (2013). The basic closures of fluid mechanics in form characteristic for the Finite Volume Method. *Technical Sciences*, 16(2), 93-107.
- Štigler, J. (2014). Analytical velocity profile in tube for laminar and turbulent flow. *Engineering Mechanics*, 21(6), 371-379. <https://doi.org/10.3390/fluids6100369>
- Weisbach, J. (1845). *Lehrbuch der Ingenieur- und Maschinen-Mechanik*, Theoretische Mechanik, Vieweg und Sohn, Braunschweig.